Acta Cryst. (1995). **B51**, 698–708

Structures of $Ta_{22}W_4O_{67}$ and $Ta_{74}W_6O_{203}$. I. Refined Structural Models using Synchrotron Radiation

BY SIEGBERT SCHMID, JOHN G. THOMPSON, A. DAVID RAE, BRENT D. BUTLER AND RAY L. WITHERS

Research School of Chemistry, Australian National University, Canberra, ACT 0200, *Australia*

NOBUO ISHIZAWA

Research Laboratory of Engineering Materials, Tokyo Institute of Technology, Nagatsuta, Midori-ku, Yokohama 226, *Japan*

AND SHUNJI KISHIMOTO

National Laboratory for High Energy Physics, Oho, Tsukuba 305, *Japan*

(*Received* 31 *January* 1994; *accepted* 11 *January* 1995)

Abstract

The crystal structures of $Ta_{22}W_4O_{67}$ [$M_r = 5788.19$, $a = 6.1485(5)$, $b = 47.6205(12)$, $c = 3.8559(3)$ Å, $\gamma = 90.04(1)°$, space group = $C112/m$ (non-standard setting), $Z = 1$, $D_x = 8.513\ g\,cm^{-3}$, $F(000) = 2438$] and $Ta_{74}W_6O_{203}$ [$M_r = 17741.06$, $a = 6.1664(5)$, $b = 29.2717(14)$, $c = 3.8731(2)$ Å, space group = *Pbam* (no. 55), $Z = 0.2$, $D_x = 8.428\ g\,cm^{-3}$, $F(000) = 1494$] were determined using synchrotron radiation at four different wavelengths below the Ta L_{III} edge [$\lambda = 1.2741$ (−146 eV), $\lambda = 1.2586$ (−26 eV), $\lambda = 1.2571$ (−14 eV) and $\lambda = 1.2563$ Å (−8 eV)]. The collection of data immediately below the Ta L_{III} edge at −8 eV enabled resolution of Ta and W of up to eight electrons, which assisted in the refinement of Ta/W ordering for both structures. Bond valence arguments have been used to locate oxygen vacancies required by the formulae. From the largest data set for $Ta_{22}W_4O_{67}$ ($\lambda = 1.2741$ Å), a final value of 0.0481 for $R_1 = \sum \|F_{obs}(h)| - |F_{calc}(h)\| / \sum |F_{obs}(h)|$ was obtained for 3082 unmerged reflections with $I(\mathbf{h}) > 3\sigma[I(\mathbf{h})]$ and for $Ta_{74}W_6O_{203}$ ($\lambda = 1.2563$ Å) a final value of 0.0571 for R_1 was obtained for 5675 unmerged reflections. The two structures are described from a conventional polyhedral perspective as 13- and 8-times superstructures occurring in the solid solution $(1-x)Ta_2O_5.xWO_3$, $0 \le x \le 0.267$.

Introduction

$Ta_{22}W_4O_{67}$ and $Ta_{74}W_6O_{203}$ are members of the solid solution $(1-x)Ta_2O_5.xWO_3$, $0 \le x \le 0.267$. $Ta_{22}W_4O_{67}$ is the W-rich end-member ($x = 0.267 = \frac{4}{15}$), whereas $Ta_{74}W_6O_{203}$ is near the middle of the solid-solution ($x = 0.14$). These compounds were originally described by Roth & Stephenson (1970) as belonging to an infinite series of anion-deficient α-UO_3-related 'line phases', the crystal structures of these compounds being derived from intergrowths of different sized α-UO_3-type units (Zachariasen, 1948; see Fig. 1).

The crystal structures of both $Ta_{22}W_4O_{67}$ and $Ta_{30}W_2O_{81}$ (the latter with composition close to $Ta_{74}W_6O_{203}$ and similarly an 8-times 'superstructure') were determined by Stephenson & Roth (1971*a*,*b*), respectively, using X-ray diffraction data (Cu $K\alpha$) from single crystals. While the positions of the heavy atoms (Ta/W) were accurately determined in each case with only slight deviation from their α-UO_3-type positions, the refined oxygen positions and occupancies were clearly implausible based on the calculation of bond-valence sums (Brown & Altermatt, 1985). Not surprisingly, Stephenson & Roth (1971*a*,*b*) were unable to distinguish between Ta and W in their refinement due to the lack of scattering contrast between these neighbouring elements.

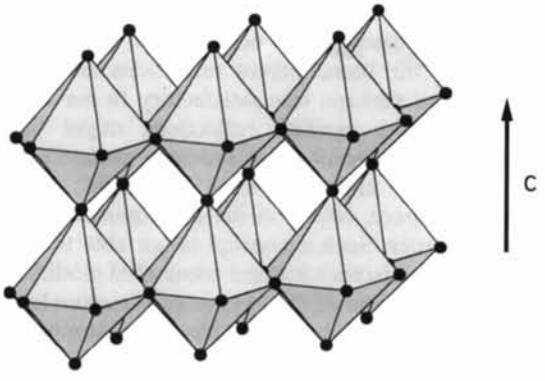

Fig. 1. The α-UO_3 structure consists of a primitive hexagonal U array with each U atom coordinated by (6 + 2) oxygens forming a hexagonal bipyramid. The hexagonal bipyramids are edge-sharing within a layer with equatorial O atoms three-coordinated by U atoms, and corner-sharing between layers with apical O atoms two-coordinate by U atoms.

More recently Schmid, Withers & Thompson (1992) have redescribed the solid solution $(1-x)Ta_2O_5.xWO_3$, $0 \leq x \leq 0.267$, as modulated variants of an average α-UO_3-type structure, whose periodicity can be either commensurate or incommensurate with respect to the average structure (*Cmmm*; $a = 6.20$–6.14, $b = 3.66$–3.65, $c = 3.89$–3.85 Å). Consequently, $Ta_{22}W_4O_{67}$ and $Ta_{30}W_2O_{81}$ were described as commensurately modulated α-UO_3-type structures with modulation wavevectors $\mathbf{q} = 8/13\ \mathbf{b}^*$ and $\mathbf{q} = 5/8\ \mathbf{b}^*$, respectively.

If one considers the solid solution in terms of the anion-deficient α-UO_3-type, it is better to express the composition as $MX_{2.577}V_{0.423} - MX_{2.5}V_{0.5}$ (M = Ta, W; X = O; V = anion vacancies). In the Stephenson & Roth (1971*a*,*b*) structures the observed anion-vacancy ordering leads to substantial relaxation of the O atoms from their ideal positions towards the vacancies, resulting in pentagonal bipyramidal (5 + 2) and distorted octahedral (4 + 2) coordination of the M atoms.

Other systems which display this anion-deficient α-UO_3-type structure are Ta_2O_5–TaO_2F in the range $MX_{2.625}$–$MX_{2.516}$ (Jahnberg & Andersson, 1967) and ZrO_2–ZrF_4 in the range $MX_{2.714}$–$MX_{2.698}$ (Thompson, Withers & Kepert, 1991). Williams, Tilley, Harburn & Williams (1991) have shown that the same structure type is also observed at the Ta_2O_5-rich end of the pseudo-binary systems with Al_2O_3, TiO_2, ZrO_2 and HfO_2.

To understand in crystal chemical terms why the crystal structure of $(1-x)Ta_2O_5.xWO_3$ is able to adapt continuously across the composition range $0 \leq x \leq 0.267$, it is necessary to obtain very accurately determined structural models which include both Ta/W ordering and oxygen vacancy distribution. Using conventional X-ray sources and 5×10^5 μm^3-sized irregular crystals, such accuracy and information is unattainable due to high absorption (*ca* 670 cm^{-1} for Mo$K\alpha$), problems with secondary extinction, poor counting statistics on weak satellite reflections, dominance of scattering by the heavy metal atoms and negligible scattering contrast between Ta and W.

For this reason we have undertaken the present study using the four-circle diffractometer on the vertical wiggler beamline 14A (BL-14A) at the Photon Factory (Satow & Iitaka, 1989) to overcome most of these problems. The collection of data immediately below the Ta L_{III} edge enables resolution of Ta and W, while the brightness of the source permits data to be collected on a sufficiently small crystal so as to minimize absorption and extinction problems, at the same time improving counting statistics on the important weak satellite reflections.

During the course of this work it became clear that $Ta_{22}W_4O_{67}$ and $Ta_{74}W_6O_{203}$ should be considered as composite modulated structures (Janner & Janssen, 1980; van Smaalen, 1991). The particular difficulties associated with the solution and refinement of such structures are treated in Part II (Rae, Schmid, Thompson, Withers & Ishizawa, 1995).

Experimental

Synthesis

Single crystals at the two compositions have been grown following principally the procedures described previously (Schmid, Withers & Thompson, 1992). Single crystals of one end-member of the solid solution field – namely $Ta_{22}W_4O_{67}$ – have been grown in the two-phase region between $Ta_{22}W_4O_{67}$ and Ta_2WO_8. A mixture of Ta_2O_5 (60 mol %) and WO_3 (40 mol %) was heated at 1873 K in a sealed platinum tube for 5 d. The resulting crystals were generally too big for use at BL-14A, therefore, a large crystal had to be cut and a small piece thereof taken for intensity measurements. This crystal approximated a square pyramid of dimensions $25 \times 25 \times 22$ μm ($V = 4 \times 10^3$ μm^3). Crystals of $Ta_{74}W_6O_{203}$ were synthesized using a stoichiometric mixture of the component oxides, *i.e.* 14 mol % WO_3, by heating the mixture in a sealed platinum tube at 1873 K for 2 d. The temperature of synthesis was well below the melting point for this composition, resulting in the production of suitably small crystals. The crystal selected for intensity measurements at BL-14A approximated a square prism of dimensions $10 \times 10 \times 12.5$ μm ($V = 1.25 \times 10^3$ μm^3).

Data collection

The quality of the crystals – magnitude of the wavevector and reflection profiles – was checked on a Rigaku AFC-6*R* four-circle diffractometer with rotating Cu anode. The crystals were mounted on tapered glass fibres with the diameter of the fibre ends being of approximately the same size as the crystals.

The data collection with synchrotron radiation was carried out on the four-circle diffractometer at a vertical wiggler port BL-14A at the Photon Factory (Satow & Iitaka, 1989). Data were collected at three different wavelengths both for $Ta_{22}W_4O_{67}$ (146, 26 and 8 eV below the Ta L_{III} absorption edge, respectively) and for $Ta_{74}W_6O_{203}$ (146, 14 and 8 eV below the edge). The important parameters for the data collection are given in Tables 1 and 2.* A Si(111) double crystal monochromator was used to monochromate the synchrotron radiation. To improve the counting statistics on weaker reflections, scans were repeated when $\sigma F/F$ was larger than 0.01, σF being calculated from counting statistics only. For $Ta_{22}W_4O_{67}$ the maximum number of scans was four, whereas for $Ta_{74}W_6O_{203}$ the maximum was three. Decay of the incident beam and spontaneous fluctuations were monitored with an ion chamber to enable normalization of the raw counts. Nine standard reflections were

* A list of observed and calculated structure factors has been deposited with the IUCr (Reference: BR0029). Copies may be obtained through The Managing Editor, International Union of Crystallography, 5 Abbey Square, Chester CH1 2HU, England.

Table 1. *Important parameters for the data collection on* $Ta_{22}W_4O_{67}$

Space group	Monoclinic, $C112/m$		
Cell dimensions			
a (Å)	6.1485 (5)		
b (Å)	47.6205 (12)		
c (Å)	3.8559 (3)		
γ (°)	90.04 (1)		
Z	1		
Density (g cm^{-3})	8.513		
Wavelength (Å)	1.2741 (−146 eV)	1.2586 (−26 eV)	1.2563 (−8 eV)
Energy (eV)	9730.6	9850.6	9868.6
Monochromator	Si(111) double crystal		
Scan mode	2θ–ω	2θ–ω	2θ–ω
Scan width (° in ω)	$0.15 + 0.02\tan\theta$ in ω		
Scan speed (° min^{-1})	1	1	1
Attenuation factor	17.9	16.0	14.4
Collimator (mm)	0.4	0.4	0.4
μ (cm^{-1})	655.69	648.05	723.38
2θ range (°)	1–140	1–110	1–110
h, k, l range	±9, ±70, ±5	+7, ±54, +4	+6, ±53, +3
No. of collected reflections	3370	1076	946
Reflections with $I > 3\sigma(I)$	3082	909	778
$\Delta f'$ (Ta)	−11.023	−14.686	−17.081
$\Delta f''$ (Ta)	3.876	3.799	3.788
$\Delta f'$ (W)	−8.616	−9.221	−9.322
$\Delta f''$ (W)	4.104	4.023	4.012
$\Delta f'$ (O)	0.031	0.030	0.030
$\Delta f''$ (O)	0.021	0.021	0.021
Overall R	0.0481	0.0354	0.0299

Table 2. *Important parameters for the data collection on* $Ta_{74}W_6O_{203}$

Space group	Orthorhombic, *Pbam* (no. 55)		
Cell dimensions			
a (Å)	6.1664 (5)		
b (Å)	29.2717 (14)		
c (Å)	3.8731 (2)		
Z	0.2		
Density (g cm^{-3})	8.428		
Wavelength (Å)	1.2741 (−146 eV)	1.2571 (−14 eV)	1.2563 (−8 eV)
Energy (eV)	9730.6	9862.6	9868.6
Monochromator	Si(111) double crystal		
Scan mode	2θ–ω	2θ–ω	2θ–ω
Scan width (° in ω)	0.4	0.4	0.4
Scan speed (° min^{-1})	16	8	8
Attenuation factor	25.0	22.0	21.0
Collimator (mm)	1.0	1.0	1.0
μ (cm^{-1})	648.06	671.08	723.55
2θ range (°)	1–110	1–70	1–138
h, k, l range	±7, −37, ±4	±5, ±26, ±3	±9, ±43, ±5
No. of collected reflections	2142	2064	7270
Reflections with $I > 3\sigma(I)$	1748	1632	5675
$\Delta f'$ (Ta)	−11.023	−15.905	−17.081
$\Delta f''$ (Ta)	3.876	3.792	3.788
$\Delta f'$ (W)	*−8.616*	*−9.286*	−9.322
$\Delta f''$ (W)	4.104	4.016	4.012
$\Delta f'$ (O)	0.031	0.030	0.030
$\Delta f''$ (O)	0.021	0.021	0.021
Overall R	0.0554	0.0610	0.0571

collected every 100 reflections in all data sets for both compositions. There was no significant change in intensity once the data had been corrected for the variation of the incident beam resulting from decay of the synchrotron ring current.

Table 3. *Merge statistics (on* F^2*)*

(*a*) $Ta_{22}W_4O_{67}$

	*m*11	1*m*1	11*m*	211	121	112	$\bar{1}$	$C112/m$
1.2741	5.71	6.05	4.40	5.68	6.06	3.95	3.45	3.98
1.2586	—	4.51	—	5.54	—	6.29	6.51	6.51
1.2563	—	5.16	—	5.88	—	6.31	6.23	6.34

(*b*) $Ta_{74}W_6O_{203}$

	*m*11	1*m*1	11*m*	211	121	112	$\bar{1}$	*Pbam*
1.2741	4.86	—	5.30	*8.27*	4.31	*8.00*	*2.17*	5.36
1.2571	5.04	4.67	6.87	5.08	4.44	5.69	2.75	6.40
1.2563	4.68	4.79	5.11	4.69	4.34	4.82	3.22	5.86

Note: Numbers in italics indicate very few reflections used.

For the $Ta_{22}W_4O_{67}$ crystal an apparent broadening of the reflection profiles with increasing θ was found, which led us to choose a scan width in ω of $0.15 + 0.02\tan\theta$. For the $Ta_{74}W_6O_{203}$ crystal a fixed scan width of 0.4° in ω was used.

The intensities were corrected for the Lorentz factor (*Xtal*3.0; Hall & Stewart, 1990). No polarization correction was applied as we assumed the beam to be perfectly polarized in the vertical plane, whereas all diffraction (monochromator crystals and four-circle diffractometer) occurred in the horizontal plane.

The data were then corrected for absorption with an analytical absorption correction, describing the crystal of $Ta_{22}W_4O_{67}$ with five faces approximating a square pyramid and $Ta_{74}W_6O_{203}$ with six faces approximating a rectangular prism. The theoretical absorption coefficients for each wavelength deduced from the program *FPRIME* (Cromer & Liberman, 1981) have been corrected using the results of our *EXAFS* experiment (see later). The merge statistics after these corrections implied a diffraction symmetry of $112/m$ for $Ta_{22}W_4O_{67}$, although the near-edge (−8 eV) data suggested that the twofold symmetry in the diffraction data may have been broken (see Table 3). For $Ta_{74}W_6O_{203}$ the merge statistics were consistent with *mmm* diffraction symmetry.

EXAFS and wavelength choice

In order to determine precisely the location of the Ta L_{III} absorption edge prior to data collection for $Ta_{22}W_4O_{67}$, two near-edge absorption spectra were collected. The first was a standard 10 μm thick Ta metal foil and the second using a fine coating of $Ta_{22}W_4O_{67}$ powder on cellophane tape. These spectra are plotted in Fig. 2. A similar near-edge absorption spectrum (not shown) was obtained using only standard 10 μm thick Ta metal foil prior to data collection on $Ta_{74}W_6O_{203}$.

In each case the location of the Ta foil absorption edge was used to provide a calibration of the indicated monochromator position with the absolute incident energy. The precision of this value is somewhat limited by the ability to define the Ta edge which spans several eV in the experimental data. We have indicated in Fig. 2 where the edge was defined in this study. It was defined

as the monochromator position that roughly corresponded to the point where Ta absorption had risen half way to its far-edge value. All other settings of the incident X-ray energy were defined relative to this indicated value. For instance, when reference is made to an energy of −8 eV, this corresponds to the monochromator step position labelled 30 (position 34 was taken as the Ta edge and each monochromator step corresponds to 2 eV). The absorption spectrum of the $Ta_{22}W_4O_{67}$ powder was taken to detect any shift in the Ta L_{III} absorption edge that might result from the +5 oxidation state of Ta in this material. By comparing the two spectra shown in Fig. 2, it is clear that the two edges are separated by at most 2 eV which is within the energy resolution of the monochromator (*ca* 2 eV).

The dispersion corrections $\Delta f'$ and $\Delta f''$ for Ta and W were calculated using the computer program *FPRIME* of Cromer & Liberman (1981). Corrections to the relativistic part of the anomalous scattering factors were made following Kissel & Pratt (1990). Very close to an absorption edge, the dispersion corrections are not known to high accuracy and so we measured the intensities of three parent and two satellite reflections for $Ta_{22}W_4O_{67}$ at ten separate incident energies as the absorption edge was approached. The decrease in the intensity of these reflections associated with the changing of $\Delta f'$ was then compared with what would be expected from theoretical calculations, so that appropriate adjustments to the dispersion corrections used during refinement of the structural models could be made. These five reflections were measured at ten energies ranging from 146 to 4 eV below the absorption edge. Large changes in the scattered intensity for these reflections were observed as the edge energy was approached. A 60% difference in integrated intensities was observed between the two energy extremes.

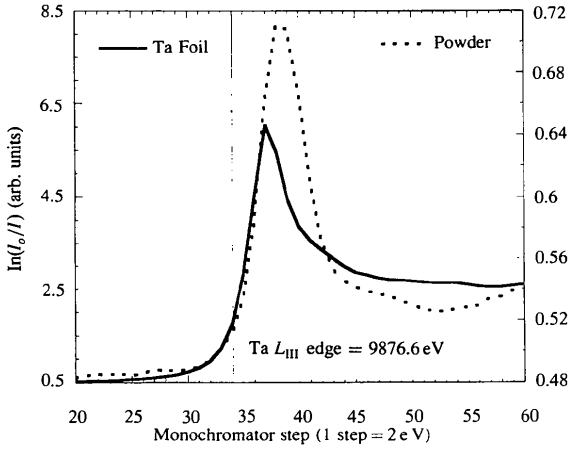

Fig. 2. Plot of absorption spectra near the Ta L_{III} absorption edge for a standard 10 μm thick Ta metal foil and a thin $Ta_{22}W_4O_{67}$ powder specimen. The derived location of the Ta L_{III} absorption edge (9876.6 eV) is shown in terms of monochromator steps.

Assuming that the value of $\Delta f'$ for Ta is accurately known at −146 eV ($\Delta f' = -11.023$; Cromer & Liberman, 1981), and that the structure of $Ta_{22}W_4O_{67}$ is known, the five derived structure factors can be used to evaluate $\Delta f'$ at all other energies. These values are plotted in Fig. 3 with the calculation of $\Delta f'$ using Cromer & Liberman's (1981) program. Since the parent structure of this material is well known, that is anion-deficient α-UO_3-type, the three parent reflections in this plot ($\bar{1}$,65,$\bar{1}$, 2,52,3 and 2,26,4) should be accurately reproduced. The two satellite reflections (5,11,1, 0,$\overline{16}$,2), however, are much more sensitive to the correctness of the refined model, and in particular the Ta/W ordering scheme.

As can be seen in Fig. 3, the measurements are in good agreement with the calculations across the range of energies. More importantly, however, all five observations of the variation of $\Delta f'$ with X-ray energy determined in this way agree closely with each other, providing further evidence that the refined structural model presented below and in Part II of this work is correct. The comparison of calculated and observed $\Delta f'$ as a function of energy was not repeated for $Ta_{74}W_6O_{203}$.

Results and discussion

The refined models

The fractional coordinates and thermal parameters for the final structural models of $Ta_{22}W_4O_{67}$ and $Ta_{74}W_6O_{203}$ are presented in Tables 4 and 5. Conventional polyhedral representations of the refined models, similar to those used by Stephenson & Roth (1971*a*, *b*, *c*), are presented in Fig. 4.

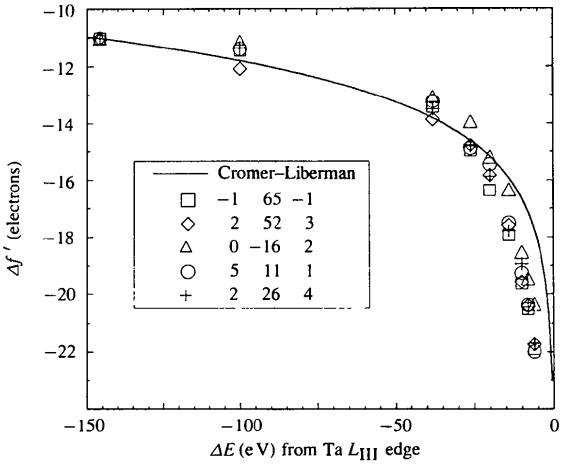

Fig. 3. Plot of the change in $\Delta f'$ with energy as the Ta L_{III} edge is approached. The experimental points were obtained from measurements of five structure factors at ten different incident X-ray energies. The intensities of three parent ($\bar{1}$,65,$\bar{1}$, 2,52,3 and 2,26,4) and two satellite (5,11,1, 0,$\overline{16}$,2) reflections were measured. Theoretical values (Cromer & Liberman, 1981) are plotted as a solid line for reference.

Table 4. *Fractional coordinates and anisotropic thermal parameters for final refined model of* $Ta_{22}W_4O_{67}$

	x	y	z	U_{11}	U_{22}	U_{33}	U_{12}
*M*1	0.0000 (–)	0.0000 (–)	0.0000 (–)	0.008 (1)	0.000 (1)	0.064 (1)	0.001 (1)
*M*2	0.5268 (1)	0.1134 (1)	0.0000 (–)	0.012 (1)	0.003 (1)	0.018 (1)	0.002 (1)
*M*3	−0.0159 (1)	0.2283 (1)	0.0000 (–)	0.010 (1)	0.007 (1)	0.007 (1)	0.002 (1)
*M*4	0.4237 (1)	0.3455 (1)	0.0000 (–)	0.009 (1)	0.005 (1)	0.004 (1)	−0.002 (1)
*M*5	−0.0500 (1)	0.4633 (1)	0.0000 (–)	0.009 (1)	0.005 (1)	0.005 (1)	−0.003 (1)
*M*6	0.5108 (1)	0.5797 (1)	0.0000 (–)	0.011 (1)	0.008 (1)	0.005 (1)	−0.005 (1)
*M*7	0.0242 (1)	0.6930 (1)	0.0000 (–)	0.007 (1)	0.002 (1)	0.061 (1)	−0.002 (1)
O1	0.0000 (–)	0.0000 (–)	0.5000 (–)	0.006 (4)	0.030 (4)	0.028 (3)	0.012 (3)
O2	0.5030 (12)	0.1107 (1)	0.5000 (–)	0.010 (3)	0.014 (2)	0.039 (2)	0.007 (2)
O3	−0.0390 (11)	0.2259 (1)	0.5000 (–)	0.005 (2)	0.012 (2)	0.017 (2)	−0.005 (2)
O4	0.4195 (10)	0.3447 (1)	0.5000 (–)	−0.001 (3)	0.009 (2)	0.009 (2)	0.002 (3)
O5	−0.0691 (12)	0.4651 (1)	0.5000 (–)	0.005 (2)	0.012 (2)	0.017 (2)	0.005 (2)
O6	0.4875 (11)	0.5827 (1)	0.5000 (–)	0.010 (3)	0.014 (2)	0.039 (2)	−0.007 (2)
O7	0.0107 (14)	0.6945 (1)	0.5000 (–)	0.006 (4)	0.030 (4)	0.028 (3)	−0.012 (3)
O8	0.2500 (–)	0.2500 (–)	0.0000 (–)	0.002 (3)	0.016 (2)	0.024 (2)	−0.002 (2)
O9	0.6799 (12)	0.3722 (1)	0.0000 (–)	0.009 (2)	0.014 (2)	0.020 (2)	−0.003 (2)
O10	0.1878 (10)	0.4940 (1)	0.0000 (–)	0.008 (2)	0.012 (1)	0.003 (1)	0.000 (2)
O11	0.6979 (12)	0.6139 (1)	0.0000 (–)	0.009 (2)	0.005 (1)	0.000 (1)	−0.001 (1)
O12	0.1346 (11)	0.7308 (1)	0.0000 (–)	0.014 (2)	0.003 (1)	0.008 (1)	−0.004 (1)
O13	0.5764 (12)	0.8461 (1)	0.0000 (–)	0.014 (3)	0.002 (2)	0.008 (2)	0.000 (1)
O14	0.0992 (14)	0.9616 (1)	0.0000 (–)	0.014 (2)	0.003 (1)	0.008 (1)	0.004 (1)
O15	0.6741 (12)	0.0771 (1)	0.0000 (–)	0.0090 (2)	0.005 (1)	0.000 (1)	0.001 (1)
O16	0.1989 (12)	0.1961 (1)	0.0000 (–)	0.008 (2)	0.012 (1)	0.003 (1)	0.000 (2)
O17	0.6729 (10)	0.3163 (1)	0.0000 (–)	0.009 (2)	0.014 (2)	0.020 (2)	0.003 (2)
O18	0.2154 (10)	0.4394 (1)	0.0000 (–)	0.002 (3)	0.016 (2)	0.024 (2)	0.002 (2)

Note: Thermal parameters for O atoms are constrained to match for pseudo-mirror-related atoms.

Table 5. *Fractional coordinates and anisotropic thermal parameters for final refined model of* $Ta_{74}W_6O_{203}$

	x	y	z	U_{11}	U_{22}	U_{33}	U_{12}
*M*1	0.7716 (1)	0.0928 (1)	0.0000 (–)	0.007 (1)	0.009 (1)	0.048 (1)	0.001 (1)
*M*2	0.2728 (1)	0.2767 (1)	0.0000 (–)	0.011 (1)	0.015 (1)	0.022 (1)	0.007 (1)
*M*3	0.7305 (1)	0.4646 (1)	0.0000 (–)	0.010 (1)	0.014 (1)	0.020 (1)	0.004 (1)
*M*4	0.1759 (1)	0.6543 (1)	0.0000 (–)	0.006 (1)	0.010 (1)	0.018 (1)	0.000 (1)
O1	0.7558 (8)	0.0887 (2)	0.5000 (–)	0.009 (2)	0.023 (2)	−0.018 (1)	0.013 (2)
O2	0.2536 (7)	0.2732 (2)	0.5000 (–)	0.012 (2)	0.022 (2)	0.006 (2)	0.009 (1)
O3	0.7131 (6)	0.4621 (1)	0.5000 (–)	0.008 (1)	0.015 (2)	0.006 (1)	0.004 (1)
O4	0.1721 (7)	0.6535 (1)	0.5000 (–)	0.014 (2)	0.012 (2)	0.007 (1)	0.001 (1)
O5	0.5000 (–)	0.0000 (–)	0.0000 (–)	0.002 (2)	0.014 (2)	0.030 (3)	0.000 (2)
O6	0.0618 (7)	0.1964 (1)	0.0000 (–)	0.007 (2)	0.035 (2)	0.016 (2)	0.009 (1)
O7	0.5768 (6)	0.3933 (1)	0.0000 (–)	0.004 (1)	0.018 (2)	0.009 (2)	0.004 (1)
O8	0.0469 (6)	0.5876 (1)	0.0000 (–)	0.002 (1)	0.012 (1)	0.012 (2)	0.004 (1)
O9	0.5583 (7)	0.7802 (1)	0.0000 (–)	0.008 (1)	0.008 (1)	0.009 (2)	0.002 (1)
O10	0.1175 (6)	0.9691 (1)	0.0000 (–)	0.008 (1)	0.010 (1)	0.014 (2)	−0.001 (1)
O11	0.6739 (7)	0.1564 (1)	0.0000 (–)	0.005 (1)	0.007 (1)	0.014 (1)	0.002 (1)

The refinement strategy and the rationale for selecting these models comprise a major part of the second paper and are not discussed here. In the present paper we have limited our data presentation and discussion to a conventional polyhedral perspective, treating $Ta_{22}W_4O_{67}$ and $Ta_{74}W_6O_{203}$ as 13- and 8-times superstructures, respectively, of the parent anion-deficient α-UO_3-type structure. These same structures are dealt with in the second paper from a modulation wave perspective.

The results obtained in this present work differ in several important ways from the previously reported structures.

(1) Use of wavelengths close to the Ta L_{III} absorption edge enabled us to determine the Ta/W ordering. Knowing this ordering proved crucial in arriving at the location of oxygen vacancies, which are required by the stoichiometry.

(2) The very high flux of synchrotron radiation on BL-14A at the Photon Factory allowed us to work with crystals sufficiently small so as to almost avoid absorption and extinction problems. The ability to tune below an absorption edge further minimized the absorption problem existing for such heavy metal oxides.

(3) The resulting high-quality data enabled us to locate the O atoms more accurately as well as resolve the correct space-group symmetries for these structures (see §4.5 of Schmid, Withers & Thompson, 1992).

Both $Ta_{22}W_4O_{67}$ and $Ta_{74}W_6O_{203}$ show an almost continuous range of metal coordination environments, from distorted octahedral (4 + 2) to regular pentagonal bipyramidal (5 + 2). This continuous variation is best monitored by considering the fifth M—O distance, the bond which transforms one to the other. These M—O distances are listed in Table 6. If for the fifth M—O distance we deem 3.0 Å to be the threshold for inclusion in the coordination polyhedron, then, for $Ta_{22}W_4O_{67}$ *M*1 and *M*7 are in distorted octahedral sites, *M*6, *M*3, *M*5 and

*M*4 are in pentagonal bipyramidal sites, with *M*2 being intermediate. In $Ta_{74}W_6O_{203}$, *M*1 is in a distorted octahedral site whereas *M*2, *M*3 and *M*4 are in pentagonal bipyramidal sites. This continuous variation in coordination polyhedra in both structures is clearly illustrated in Fig. 4.

Interestingly, the refined Ta/W ordering (see Table 6 and Table 6 of Part II) correlates directly with the coordination environment, *i.e.* W prefers the distorted octahedral sites. In $Ta_{22}W_4O_{67}$, the majority of the W is located on the distorted octahedral sites *M*1 and *M*7 with a rather smaller amount on sites *M*2 and *M*6. Note that Ta plus W occupancy on any one metal atom site always equals 1. In $Ta_{74}W_6O_{203}$, all the W is located on *M*1, *i.e.* the *M*1 site has 30% W occupancy.

If one considers the coordination of O atoms in the plane of the metal atoms, *i.e.* at $z = 0$, there is a corresponding continuum from linear two-coordinate sites, O8 in $Ta_{22}W_4O_{67}$ and O5 in $Ta_{74}W_6O_{203}$ to regular three-coordinate sites, *e.g.* O15 and O11 in $Ta_{22}W_4O_{67}$ and O9 in $Ta_{74}W_6O_{203}$ (see Fig. 5).

Table 6. *Description of polyhedron for metal atoms*

	%W on site	$d_{(M-O)}$ in plane				Fifth bond
$Ta_{22}W_4O_{67}$						
*M*1	0.58 (2)	—O10	—O14	—O10	—O14	—O18
		1.939 (6)	1.925 (4)	1.939 (6)	1.925 (4)	3.372 (6)
*M*7	0.55 (2)	—O13	—O16	—O12	—O17	—O8
		1.962 (4)	2.004 (7)	1.921 (4)	1.913 (6)	3.191 (1)
*M*2	0.09 (2)	—O11	—O13	—O9	—O15	—O18
		2.020 (7)	2.030 (3)	1.929 (7)	1.949 (5)	2.919 (6)
*M*6	0.08 (2)	—O11	—O18	—O14	—O15	—O9
		1.991 (5)	1.912 (7)	2.079 (4)	2.072 (7)	2.572 (5)
*M*3	0.0	—O12	—O12	—O8	—O16	—O17
		2.078 (4)	2.151 (7)	1.933 (1)	2.023 (6)	2.332 (5)
*M*5	0.0	—O18	—O15	—O14	—O10	—O10
		1.988 (6)	2.068 (4)	2.157 (9)	2.066 (5)	2.201 (5)
*M*4	0.0	—O11	—O9	—O17	—O16	—O13
		2.075 (4)	2.023 (6)	2.065 (5)	2.114 (4)	2.134 (7)
$Ta_{74}W_6O_{203}$						
*M*1	0.30 (2)	—O8	—O11	—O7	—O10	—O5
		1.970 (4)	1.955 (3)	1.925 (4)	1.937 (4)	3.192 (1)
*M*2	0.0	—O9	—O11	—O9	—O6	—O6
		2.044 (4)	2.053 (3)	1.948 (4)	1.964 (3)	2.685 (4)
*M*3	0.0	—O10	—O10	—O5	—O8	—O7
		2.062 (4)	2.151 (4)	1.958 (1)	2.054 (4)	2.293 (4)
*M*4	0.0	—O9	—O6	—O7	—O8	—O11
		2.049 (3)	2.034 (4)	2.065 (4)	2.107 (4)	2.158 (4)

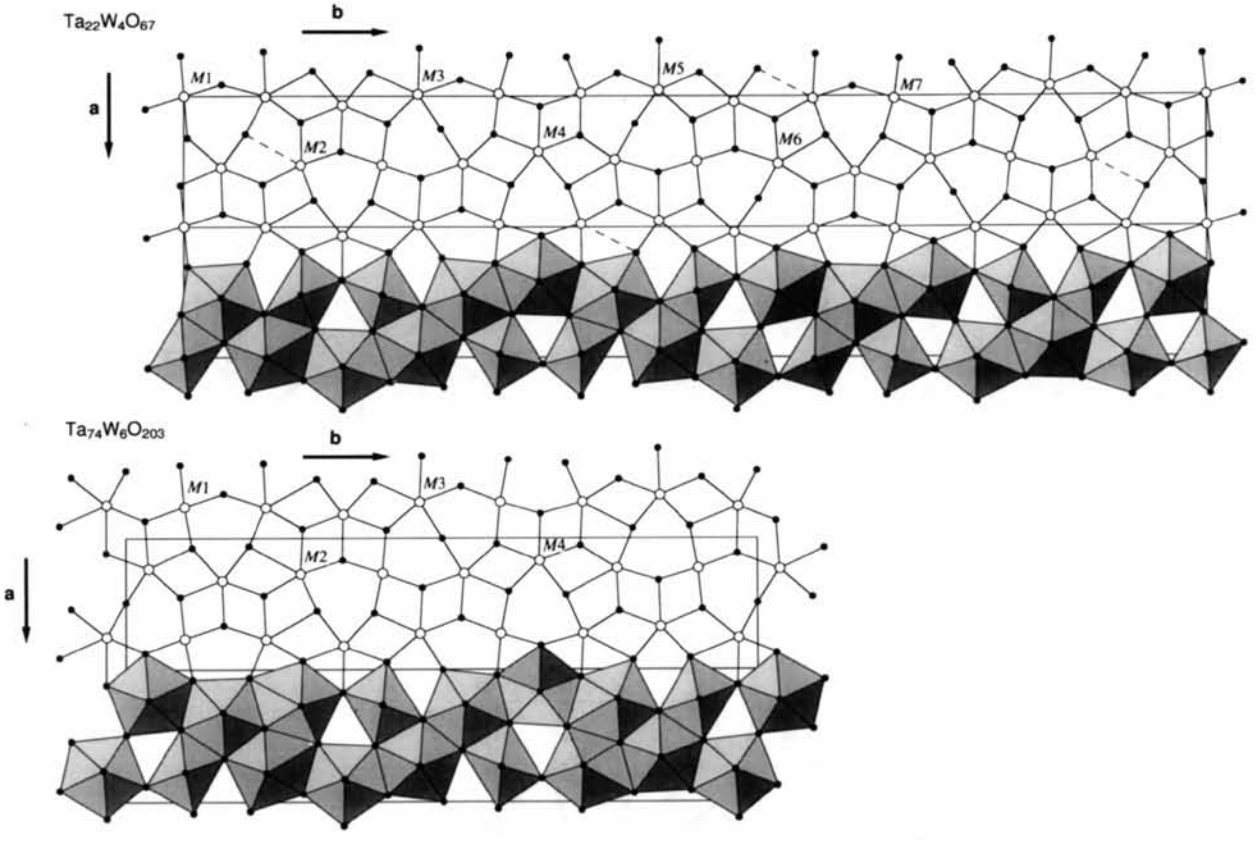

Fig. 4. *c*-Axis projection of the refined structures of $Ta_{22}W_4O_{67}$ and $Ta_{74}W_6O_{203}$ with the metal atom sites labelled. The unit cells ($a = 6.1485$, $b = 47.6205$ Å for $Ta_{22}W_4O_{67}$ and $a = 6.1664$, $b = 29.2717$ Å for $Ta_{74}W_6O_{203}$) are outlined. The two projections are aligned in the horizontal direction to emphasize the close relationship between the structures. Both structures are also presented in terms of polyhedra showing the continuous variation from distorted octahedral to almost regular pentagonal bipyramidal. This trend is best observed by following the vector $13\mathbf{a} + 3\mathbf{b}$ in $Ta_{22}W_4O_{67}$ and $8\mathbf{a} + 3\mathbf{b}$ in $Ta_{74}W_6O_{203}$.

Anion vacancy distribution

In both the refined models there is a discrepancy between the stoichiometries implied by full occupancy of all the refined atomic positions, $M_{26}O_{68}$ and $M_{80}O_{210}$, and those required by charge balance, *i.e.* $Ta_{22}W_4O_{67}$ and $Ta_{74}W_6O_{203}$. Stephenson & Roth (1971*a*, *b*) were also aware of this problem and proposed, on the basis of their refinements, partial occupancy of oxygen sites in the metal plane. In the case of $Ta_{22}W_4O_{67}$ one oxygen vacancy per formula unit was required. This led to very complicated, and necessarily disordered, chemical environments for Ta/W atoms adjacent to these vacancies. As the occupancy of oxygen sites is effectively unrefinable, even for synchrotron data, one must seek indirect evidence for the location of the oxygen vacancies. This evidence is provided by the calculation of apparent valences (AV's), *i.e.* bond-valence sums (Brown & Altermatt, 1985).

Let us consider $Ta_{22}W_4O_{67}$ first. Table 7 lists AV's calculated for the metal sites in the final structure using *EUTAX*1 (Brese & O'Keeffe, 1991). As described above, the majority of the W atoms are located on the distorted octahedral sites *M*1 and *M*7 with a much smaller W occupancy on sites *M*2 and *M*6. The AV's indicate that any Ta located at the *M*1 and *M*7 sites would be heavily overbonded, whereas Ta located at any other sites (except perhaps *M*2) would be reasonably bonded. Similarly the AV's indicate that any W located on the *M*1 and *M*7 sites would be satisfactorily bonded, whereas any W located on the *M*2 and *M*6 sites would be heavily underbonded. Accommodating W on the *M*2 and *M*6 sites would require some local rearrangement of the surrounding oxygens consistent with maintaining the average local environment obtained from the refinement. One way of accommodating Ta on the most W-favourable *M*1 and *M*7 sites would be to introduce an oxygen vacancy at the apical oxygen sites, O1 and O7, between a pair of Ta atoms. For a *c*-axis string with an idealized W occupancy of $\frac{2}{3}$, the resulting composition would be $[-W-O]_{0.8}[-Ta\ V\ Ta-O]_{0.2}$. Theoretically it might be possible to order exactly such strings along **c**. If this was the case, one might expect to see superstructure

Table 7. *Apparent valences* (AV's) *for* $Ta_{22}W_4O_{67}$

Site	*M*1	*M*2	*M*3	*M*4	*M*5	*M*6	*M*7				
Ta	4.88	5.36	5.16	5.22	5.11	5.24	4.69				
W	5.87	5.37	—	—	—	5.26	5.68				
Site	O1	O2	O3	O4	O5	O6	O7				
	1.96	1.91	1.92	1.96	1.93	1.91	1.95				
Site	O8	O9	O10	O11	O12	O13	O14	O15	O16	O17	O18
	1.93	1.91	2.09	2.25	2.19	2.20	2.17	2.26	2.14	2.02	1.92

$R_0W-O = 1.921$; $R_0Ta-O = 1.920$.

Note: The AV's are calculated using the final refined model for the structure, *i.e.* Ta on *M*1 and *M*7 incurs one oxygen vacancy and is therefore fivefold (4 + 1) coordinated. W on these sites is sixfold (4 + 2) coordinated, whereas Ta on positions *M*2–*M*6 and W on positions *M*2 and *M*6 are sevenfold (5 + 2) coordinated. The virtually identical R_0 parameters indicate that the AV's for the O atoms do not depend on the neighbouring metal site occupancy.

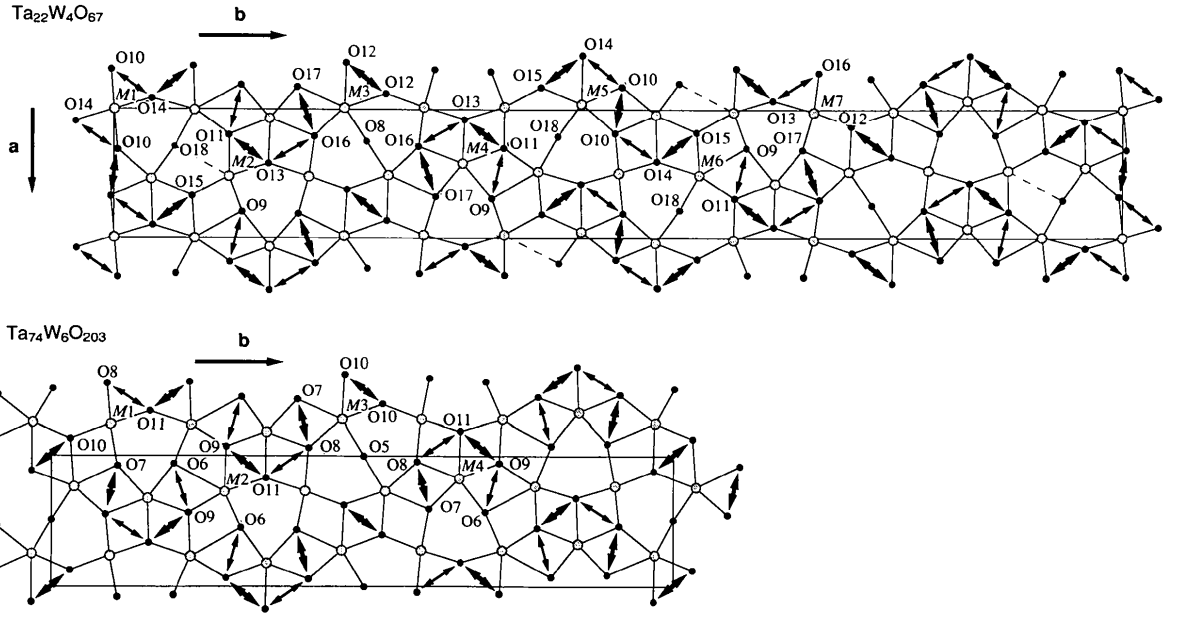

Fig. 5. *c*-Axis projection of the refined structures of $Ta_{22}W_4O_{67}$ and $Ta_{74}W_6O_{203}$ with the in-plane oxygen atom sites labelled. The unit cells ($a = 6.1485$, $b = 47.6205$ Å for $Ta_{22}W_4O_{67}$ and $a = 6.1664$, $b = 29.2717$ Å for $Ta_{74}W_6O_{203}$) are outlined. They are aligned in the horizontal direction to emphasize their close structural relationship. Double-headed arrows indicate short O—O distances (heavier arrows $d_{O-O} < 2.4$ Å; lighter arrows $2.4 \leq d_{O-O} < 2.5$ Å).

reflections along **c***. However, electron diffraction patterns for this material do not display evidence for an ordered superstructure. Instead, there is a rather diffuse sheet of intensity normal to **c*** at *ca* $\pm\frac{1}{12}$ **c*** (see Fig. 6). While this diffuse intensity can be interpreted in terms of correlated *c*-axis motion of atoms (see below), its reciprocal dimension does not appear to be related to metal and/or vacancy ordering along the *c*-axis strings.

Now let us consider $Ta_{74}W_6O_{203}$. Table 8 lists AV's calculated for the metal sites in the final structure using *EUTAX*1 (Brese & O'Keeffe, 1991). 30% occupancy of the distorted octahedral *M*1 site by W satisfies the stoichiometry. As for $Ta_{22}W_4O_{67}$, the AV's indicate that the Ta located at the *M*1 site would be significantly overbonded if it was six-coordinate by oxygen. Again, the Ta on these W-favourable sites can be accommodated by introducing an oxygen vacancy at the apical oxygen site O1 between a pair of Ta atoms. This satisfies stoichiometry. The resulting composition along such a *c* axis string would be $[-W-O]_{0.462}[-Ta\ V\ Ta-O]_{0.538}$.

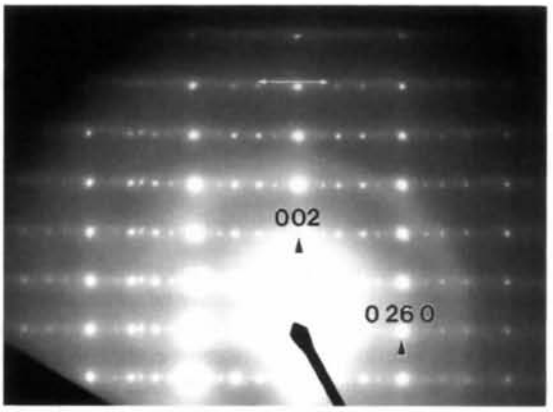

(*a*)

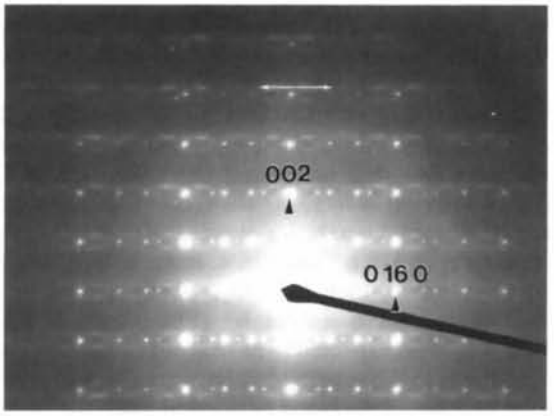

(*b*)

Fig. 6. Selected-area electron diffraction patterns down the [100] zone-axis for (*a*) $Ta_{22}W_4O_{67}$ and (*b*) $Ta_{74}W_6O_{203}$, showing the approximately continuous sheets of diffuse intensity normal to the **c*** directions at about $\pm 1/12$ **c*** for $Ta_{22}W_4O_{67}$ and about $\pm 1/8$ **c*** for $Ta_{74}W_6O_{203}$.

Table 8. *Apparent valences* AV's *for* $Ta_{74}W_6O_{203}$

Site	*M*1	*M*2	*M*3	*M*4			
	4.67	5.24	5.07	5.15			
	5.66	—	—	—			
Site	O1	O2	O3	O4			
	1.88	1.88	1.89	1.91			
	1.89	—	—	—			
Site	O5	O6	O7	O8	O9	O10	O11
	1.81	1.79	2.03	2.17	2.31	2.17	2.13
	—	—	2.03	2.18	—	2.18	2.14

R_0W—O = 1.921; R_0Ta—O = 1.920.

Note: The AV's are calculated using the final refined model for the structure, *i.e.* Ta on *M*1 incurs one oxygen vacancy and is therefore fivefold (4 + 1) coordinated. W on this site is sixfold (4 + 2) coordinated, whereas Ta on positions *M*2–*M*4 is sevenfold (5 + 2) coordinated The virtually indentical R_0 parameters indicate that the AV's for the oxygen atoms do not depend on the neighbouring metal site occupancy.

Electron diffraction patterns of $Ta_{74}W_6O_{203}$ show sheets of diffuse intensity normal to **c*** at about $\pm 1/8$ **c*** (Fig. 6). The difference in the location of this diffuse intensity compared with that observed for $Ta_{22}W_4O_{67}$ indicates that this diffraction feature is composition dependent.

As described previously (Schmid, Withers & Thompson, 1992), the non-uniform distribution of intensity of the diffuse sheets, such that more intensity occurs along **c*** than normal to this direction (Fig. 6), is consistent with displacement of atoms from the mirror planes along the *c* axis. The introduction of vacancies into the *c*-axis strings would undoubtedly cause such displacement that the strings relax to optimize bonding requirements. This postulated displacement is further supported by the large U_{33}'s on *M*1 and *M*7 for $Ta_{22}W_4O_{67}$ (see Table 4) and on *M*1 for $Ta_{74}W_6O_{203}$ (see Table 5), corresponding to mean shifts of 0.25 and 0.22 Å, respectively, from the mirror.

High-resolution TEM images of the closely related $17.5\,Ta_2O_5{:}1TiO_2$ along the [100] zone axis (Harburn, Tilley, Williams, Williams & Hutchison, 1992) revealed dark contrast linking the 3.8 Å fringes corresponding to the metal–oxygen layers. It is possible that this dark contrast results from vacancy ordering with associated metal displacement along the *c* direction, similar to that described above for the solid solution $(1-x)Ta_2O_5.xWO_3$, $0 \le x \le 0.267$.

Apparent valences and non-bonded atomic distances for the final model

The apparent valences (*EUTAX*1; Brese & O'Keeffe, 1991) for all atomic sites in the final refined model, taking into account the refined Ta/W ordering and oxygen vacancy distribution, are given in Tables 7 and 8. Compared with the previously reported structures (Stephenson & Roth, 1971*a*,*b*), the AV's are in much better agreement with the expected valences.

In $Ta_{22}W_4O_{67}$ the pentagonal bipyramidal metal sites *M*3–*M*5, which are occupied by Ta, are all within 5% of

their expected valence of +5. The distorted octahedral sites, *M*1 and *M*7, give AV's of 4.88 and 4.69, respectively, for Ta and 5.87 and 5.68, respectively, for W. The average AV's for these two sites are 5.46 and 5.23, respectively, compared with an expected valence based on composition and postulated oxygen vacancy distribution of 5.58 and 5.55, respectively. The remaining intermediate sites, *M*2 and *M*6, calculate at 5.36 and 5.25 compared with expected valences of 5.09 and 5.08. It should be remembered that the AV's are calculated for the average $Ta_{22}W_4O_{67}$ structure, which does not take into account the displacive disorder associated with the local presence or absence of oxygen vacancies. Displacement of *M*1 and *M*7 along the *c* axis, *i.e.* off the mirror plane, implied by the large U_{33}'s for these sites, may well remedy these discrepancies locally.

In $Ta_{74}W_6O_{203}$ the pentagonal bipyramidal metal sites *M*2–*M*4, which are occupied by Ta, are again all within 5% of their expected valence of +5. The distorted octahedral site, *M*1, which is 30% occupied by W, has an average AV of 4.97, compared with an expected value of 5.30. As for $Ta_{22}W_4O_{67}$, relaxation of *M*1 off the mirror along the *c* axis, implied by the large U_{33} for this site, may account for the apparent underbonding.

For both structures the O atoms can be treated in two groups – the apical O atoms which are all slightly underbonded, and the in-plane oxygens, most of which are satisfactorily bonded or somewhat overbonded. The only significantly overbonded O atoms are in-plane oxygens O11 and O15 in $Ta_{22}W_4O_{67}$ and O9 in $Ta_{74}W_6O_{203}$. It is noteworthy that these oxygens are the most regular of the three-coordinate anion sites.

In such metal oxide structures a further check on the plausibility of the structural model is gained by consideration of non-bonded atomic distances. In both structures the only 'short' distances are O—O interactions in the metal plane, *i.e.* around the equator of the metal-based polyhedra. Table 9 lists these distances. If, as before (Schmid, Withers & Thompson, 1992), we consider *ca* 2.5 Å as a minimum acceptable O—O distance in such metal oxide structures, we find that about half such interactions are less than this minimum distance. Fig. 5 presents these interactions visually for both structures with lighter double-headed arrows, indicating $2.4 \leq d_{O-O} < 2.5$ Å, the heavier arrows representing distances < 2.4 Å.

There is a possible explanation as to why these structures cannot alleviate these short O—O distances. The O atoms which have these short distances have in common that they are satisfactorily bonded or that they are overbonded and regular three-coordinate. These O atoms would be able to increase their non-bonded distances by relaxation away from the close neighbour, but this would only exacerbate the overbonding of that oxygen. This is because of the exponential relationship between bond-valence and bond-length, such that the AV is minimized when all three *M*—O bonds are equal. Any deviation from the centre necessarily increases the AV. As a result, the three-coordinate in-plane O atoms remain in these positions which represent a compromise, simultaneously reducing non-bonded interactions and minimizing overbonding.

Table 9. *Description of polyhedra for metal atoms*

Atom	%W on site	$d_{(O-O)}$ around equator				
$Ta_{22}W_4O_{67}$						
*M*1	0.58 (2)	O10	O14	O10	O14	O10
		2.484 (8)	2.960 (9)	2.484 (8)	2.960 (9)	
*M*7	0.55 (2)	O13	O16	O12	O17	O13
		2.435 (7)	3.146 (7)	2.536 (7)	2.854 (9)	
*M*2	0.09 (2)	O11	O13	O9	O15	O18	O11
		2.356 (8)	2.734 (9)	2.575 (6)	2.518 (10)	2.590 (6)
*M*6	0.08 (2)	O11	O18	O14	O15	O9	O11
		2.590 (6)	2.584 (10)	2.309 (8)	2.575 (6)	2.414 (9)
*M*3	0.0	O12	O12	O8	O16	O17	O12
		2.312 (11)	2.533 (7)	2.586 (4)	2.359 (8)	2.536 (7)
*M*5	0.0	O18	O15	O14	O10	O10	O18
		2.518 (10)	2.309 (8)	2.484 (9)	2.377 (12)	2.604 (6)
*M*4	0.0	O11	O9	O17	O16	O13	O11
		2.414 (9)	2.657 (7)	2.359 (8)	2.435 (7)	2.356 (8)
$Ta_{74}W_6O_{203}$						
*M*1	0.30 (2)	O8	O11	O7	O10	O8	
		2.429 (5)	2.878 (6)	2.522 (5)	3.124 (6)	
*M*2	0.0	O9	O11	O6	O9	O6	O9
		2.344 (5)	2.664 (6)	2.562 (5)	2.440 (5)	2.562 (5)
*M*3	0.0	O10	O10	O5	O8	O7	O10
		2.318 (7)	2.526 (4)	2.581 (4)	2.387 (6)	2.522 (5)
*M*4	0.0	O9	O6	O7	O8	O11	O9
		2.562 (5)	2.628 (6)	2.387 (6)	2.429 (5)	2.344 (5)

The relationship between periodicity and composition

The periodicity, or wavevector magnitude in modulated structure terms, for continuously adaptive structures can usually be considered as a 'chemical ruler', *i.e.* there is a direct relationship between composition and wavevector magnitude. Examples of such structures are $Nb_2Zr_{x-2}O_{2x+1}$: $x = 7.1$–10.3 (Thompson, Withers, Sellar, Barlow & Hyde, 1990) and $ZrO_{2-x}F_{2x}$: $0.698 \leq x \leq 0.714$ (Thompson, Withers & Kepert, 1991). In the present case, namely $(1-x)Ta_2O_5.xWO_3$, $0 \leq x \leq 0.267$, this is not so. The wavevector relates to only the ratio of *M* atoms to in-plane O atoms. It is this ratio which determines the proportion of metal sites which have distorted octahedral character. $Ta_{22}W_4O_{67}$ with wavevector $\mathbf{q} = 8/13\ \mathbf{b}^*$ has 6 out of 26 metal sites which are distorted octahedra, whereas $Ta_{74}W_6O_{203}$ with wavevector $\mathbf{q} = 5/8\ \mathbf{b}^*$ has 1 in 4. If we assume this is a linear relationship, then *L*-Ta_2O_5, which is reported to have a wavevector $\mathbf{q} = 7/11\ \mathbf{b}^*$ (Stephenson & Roth, 1971*c*), would be expected to have 6 out of 22 such sites.

In addition to the relationship between the wavevector and the number of distorted octahedral sites, the present structure refinements indicate that W prefers to occupy these distorted octahedral sites. This is supported by bond-valence calculations and observed U_{33}'s which also suggest that apical oxygen vacancies are associated with Ta in distorted octahedral sites.

We can summarize the above relationships if we rewrite the formulae as follows

$Ta_{22}W_4O_{67} \rightarrow M_{26}O(\text{apical})_{25}O(\text{in-plane})_{42} \rightarrow$
$Ta(\text{pentagonal})_{20/26}Ta(\text{dist. oct.})_{2/26}W_{4/26}$-
$O(\text{apical})_{25/26}\ O(\text{in-plane})_{1+q}(\mathbf{q} = 8/13\,\mathbf{b}^*)$

$Ta_{74}W_6O_{203} \rightarrow M_{80}O(\text{apical})_{73}O(\text{in-plane})_{130} \rightarrow$
$Ta(\text{pentagonal})_{60/80}Ta(\text{dist. oct.})_{14/80}W_{6/80}$-
$O(\text{apical})_{73/80}O(\text{in-plane})_{1+q}(\mathbf{q} = 5/8\,\mathbf{b}^*)$

$Ta_2O_5 \rightarrow Ta_{22}O_{55} \rightarrow M_{22}O(\text{apical})_{19}O(\text{in-plane})_{36} \rightarrow$
$Ta(\text{pentagonal})_{16/22}Ta(\text{dist. oct.})_{6/22}O(\text{apical})_{19/22}$
$O(\text{in-plane})_{1+q}(\mathbf{q} = 7/11\,\mathbf{b}^*)$.

The generalization of these formulae is discussed further in Part II of this work.

Knowing the proportion of distorted octahedral metal sites still does not give us the W/Ta ratio. This is because of the further degree of freedom such that [–Ta V Ta–O] can substitute continuously for [–W–O–W–O] on such sites. In theory, for any given wavevector, there is a possible range of compositions. In practice, there appears to be a unique Ta/W ratio for a given wavevector at a given temperature of synthesis. For example, Stephenson & Roth (1971*b*) observed a wavevector of $\mathbf{q} = 5/8\,\mathbf{b}^*$ for $Ta_{30}W_2O_{81}$ for material grown at 2033 K, whereas we observe the same wavevector at the more W-rich composition $Ta_{74}W_6O_{203}$, , the only difference being that our material was annealed at 1873 K. Our earlier work showed that there is in fact a linear relationship between W content and wavevector for specimens prepared at 1873 K (Schmid, Withers & Thompson, 1992).

From our rewriting of the formulae given above, it is evident that the proportion of distorted octahedral sites decreases with increasing W content. For $Ta_{74}W_6O_{203}$, all W is located on the distorted octahedral ($M1$) site. For

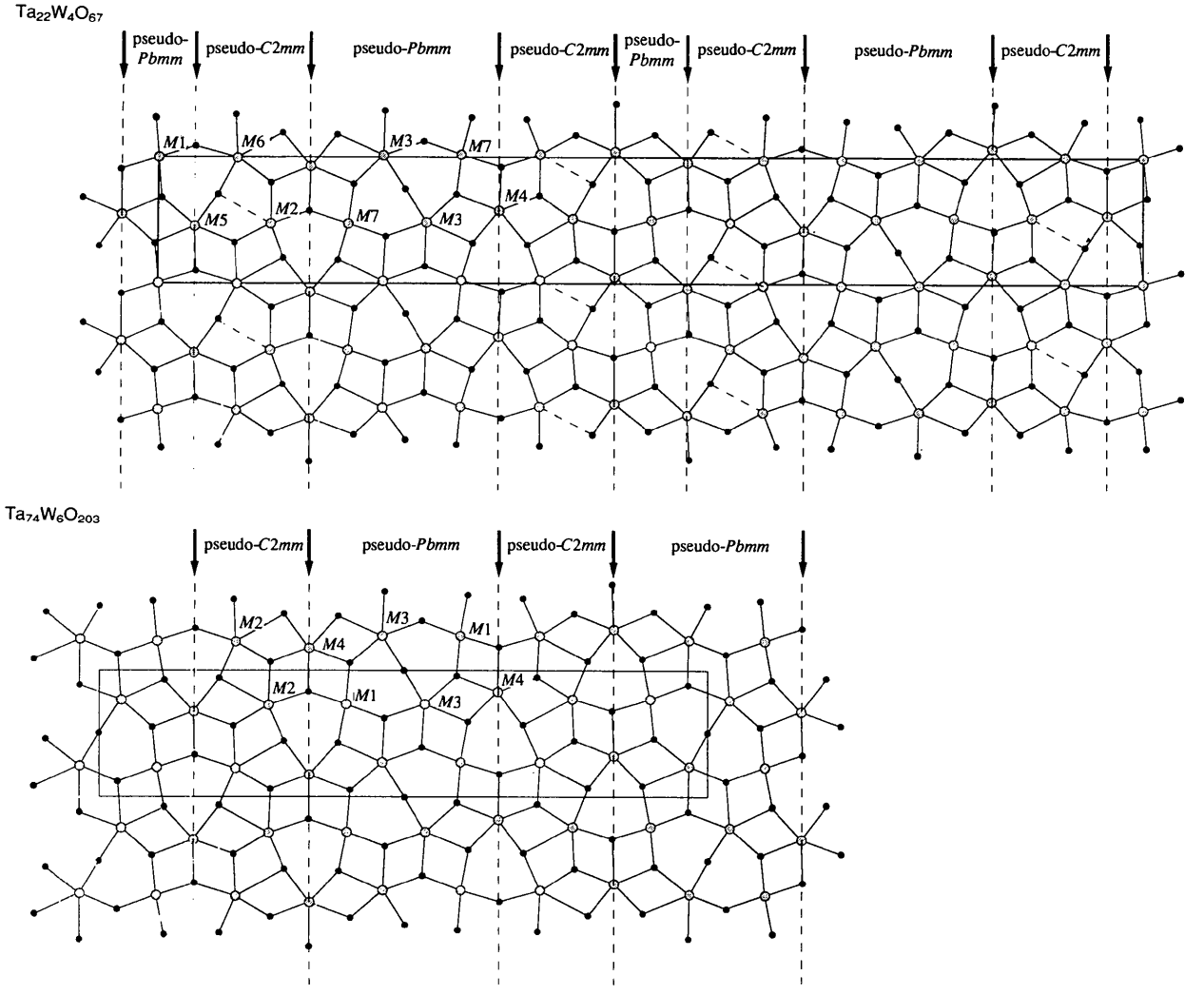

Fig. 7. Projection down **c*** of the $Ta_{22}W_4O_{67}$ and $Ta_{74}W_6O_{203}$ structures. These refined modulated structures can be approximated as regions or strips of structure, delineated by pseudo-mirror planes (dashed lines). The approximate symmetry of these regions or strips is apparent.

$Ta_{22}W_4O_{67}$, most of the W's are still located on the distorted octahedral (*M*1 and *M*7) sites. However, it appears that a small but significant amount of W is located on the less favourable, more pentagonal bipyramidal in character (*M*2 and *M*6) sites. It can therefore be assumed that the end-member composition ($x = 0.267$) is determined by the maximum amount of W that can be accommodated on these less favourable sites.

Description of structures in terms of 'strips'

To try to distinguish the different types of chemical environments that occur throughout the solid solution, the crystal structures can be approximated as consisting of strips of structure perpendicular to **b** with pseudo-*Pbmm* and pseudo-*C*2*mm* symmetry. The width of the pseudo-*C*2*mm* strips is invariant while the width of the pseudo-*Pbmm* strips varies as a function of the composition x in $(1-x)Ta_2O_5.xWO_3$ (see Fig. 7). If we define f as the fraction of the *M* sites which are distorted octahedral sites, $f = (2b_M/b_O) - 3$ (see Part II), then it holds for all compositions that $2f$ sites are pentagonal bipyramidal and that $1–3f$ sites are transitional, *i.e.* their geometries are intermediate between distorted octahedral and regular pentagonal bipyramidal. The only sites which occur within the pseudo-*C*2*mm* strips are the transitional sites, *i.e.* *M*2 and *M*6 in $Ta_{22}W_4O_{67}$ and *M*2 in $Ta_{74}W_6O_{203}$, whereas both the distorted octahedral sites and regular pentagonal bipyramidal sites occur within the pseudo-*Pbmm* strips, or on the pseudo-mirror planes delineating the strips (indicated by dashed lines in Fig. 7). In the middle of both the pseudo-*Pbmm* and pseudo-*C*2*mm* strips, there also exist pseudo-*a*-glide planes perpendicular to **b**.

The composition of the pseudo-*C*2*mm* strips is M_3O_8 if one assumes no apical oxygen vacancies are associated with the transitional sites. The composition of the pseudo-*Pbmm* strips is, in the general case, $M_{3n-1}O_{8n-3}$, $n = 1, 2, 3\ldots$, if one ignores the oxygen vacancies associated with the distorted octahedral sites. $Ta_{74}W_6O_{203}$ consists of pseudo-*Pbmm* strips where $n = 2$ only, whereas $Ta_{22}W_4O_{67}$ consists of pseudo-*Pbmm* strips which are alternately $n = 1$ and $n = 2$. In these terms, the continuous variation in stoichiometry across the solid solution can be understood as continuously varying the volume of the pseudo-*Pbmm* strips relative to the volume of the pseudo-*C*2*mm* strips. The proportion of distorted octahedral sites, *i.e.* sites capable of accommodating W, will increase as the relative volume of the pseudo-*Pbmm* strips increases. The theoretical limiting cases, according to this description, will be where the pseudo-*Pbmm* strips are all $n = 1$ or where $n \rightarrow \infty$. In practice, the range is limited to alternating $n = 1$ and 2 in $Ta_{22}W_4O_{67}$ as one end-member and all $n = 3$ for *L*-Ta_2O_5 as the other.

Financial support of the Australian National Beamline Facility is acknowledged. The ANBF is funded by a consortium comprising the ARC, DITARD, ANSTO, CSIRO, ANU and UNSW. We also thank the National Laboratory for High Energy Physics, Tsukuba, for the generous allocation of beam time (Project No. 92-096). The assistance of S'da Katsumi was invaluable in collecting the diffraction data at the Photon Factory and is greatly appreciated.

References

BRESE, N. E. & O'KEEFFE, M. (1991). *Acta Cryst.* B**47**, 192–197.

BROWN, I. D. & ALTERMATT, D. (1985). *Acta Cryst.* B**41**, 244–247.

CROMER, D. T. & LIBERMAN, D. A. (1981). *Acta Cryst.* A**37**, 267–268.

HALL, S. R. & STEWART, J. M. (1990). Editors. *Xtal*3.0 *Reference Manual*. Univs. of Western Australia, Australia, and Maryland, USA.

HARBURN, G., TILLEY, R. J. D., WILLIAMS, J. M., WILLIAMS, R. P. & HUTCHISON, J. (1992). *J. Chem. Soc. Faraday Trans.* **88**, 621–624.

JAHNBERG, L. & ANDERSSON, S. (1967). *Acta Chem. Scand.* **21**, 615–619.

JANNER, A. & JANSSEN, T. (1980). *Acta Cryst.* A**36**, 408–415.

KISSEL, L. & PRATT, R. H. (1990). *Acta Cryst.* A**46**, 170–175.

RAE, A. D., SCHMID, S., THOMPSON, J. G., WITHERS, R. L. & ISHIZAWA, N. (1995). *Acta Cryst.* B**51**, 709–721.

ROTH, R. S. & STEPHENSON, N. C. (1970). *Chemistry of Extended Defects in Non-Metallic Solids*, edited by L. EYRING & M. O'KEEFFE, pp. 167–182. Amsterdam: North-Holland Publishing Company.

SATOW, Y. & IITAKA, Y. (1989). *Rev. Sci. Instrum.* **60**, 2390–2393.

SCHMID, S., WITHERS, R. L. & THOMPSON, J. G. (1992). *J. Solid State Chem.* **99**, 226–242.

SMAALEN, S. VAN (1991). *Phys. Rev. B*, **43**, 11330–11341.

STEPHENSON, N. C. & ROTH, R. S. (1971*a*). *Acta Cryst.* B**27**, 1010–1017.

STEPHENSON, N. C. & ROTH, R. S. (1971*b*). *Acta Cryst.* B**27**, 1018–1024.

STEPHENSON, N. C. & ROTH, R. S. (1971*c*). *Acta Cryst.* B**27**, 1037–1044.

THOMPSON, J. G., WITHERS, R. L. & KEPERT, C. J. (1991). *J. Solid State Chem.* **95**, 111–125.

THOMPSON, J. G., WITHERS, R. L., SELLAR, J., BARLOW, P. J. & HYDE, B. G. (1990). *J. Solid State Chem.* **88**, 465–475.

WILLIAMS, J. M., TILLEY, R. J. D., HARBURN, G. & WILLIAMS, R. P. (1991). *J. Solid State Chem.* **92**, 460–472.

ZACHARIASEN, W. H. (1948). *Acta Cryst.* **1**, 265–268.